THE JOURNAL OF PHYSICAL CHEMISTRY Letters

This is an open access article published under a Creative Commons Attribution (CC-BY) License, which permits unrestricted use, distribution and reproduction in any medium, provided the author and source are cited.

ACS AUTHORCHOICE

pubs.acs.org/JPCL

Letter

Enabling Natural Abundance ^{17}O Solid-State NMR by Direct Polarization from Paramagnetic Metal Ions

Daniel Jardón-Álvarez, Guy Reuveni, Adi Harchol, and Michal Leskes*

Cite This: *J. Phys. Chem. Lett.* 2020, 11, 5439−5445

Read Online

ACCESS | Metrics & More | Article Recommendations | Supporting Information

ABSTRACT: Dynamic nuclear polarization (DNP) significantly enhances the sensitivity of nuclear magnetic resonance (NMR), increasing its applications and the quality of NMR spectroscopy as a characterization tool for materials. Efficient spin diffusion among the nuclear spins is considered to be essential for spreading the hyperpolarization throughout the sample, enabling large DNP enhancements. This scenario mostly limits the polarization enhancement of low-sensitivity nuclei in inorganic materials to the surface sites when the polarization source is an exogenous radical. In metal-ion-based DNP, the polarization agents are distributed in the bulk sample and act as a source of both relaxation and polarization enhancement. We have found that as long as the polarization agent is the main source of relaxation, the enhancement does not depend on the distance between the nucleus and dopant. As a consequence, the requirement of efficient spin diffusion is lifted, and the entire sample can be directly polarized. We exploit this finding to measure high-quality NMR spectra of ^{17}O in the electrode material $Li_4Ti_5O_{12}$ doped with Fe(III) despite its low abundance and long relaxation time.

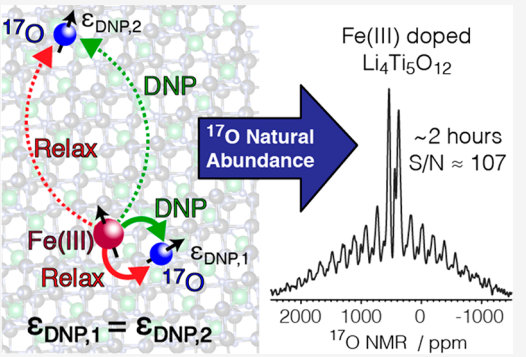

Downloaded via 79.177.9.122 on June 25, 2020 at 19:46:08 (UTC).
See https://pubs.acs.org/sharingguidelines for options on how to legitimately share published articles.

The development of inorganic materials with new functionalities or improved properties requires deep understanding of the relevant physicochemical properties. Solid-state nuclear magnetic resonance (NMR) spectroscopy is likely the most powerful method for characterizing the local structure of materials.[1,2] Parameters accessible from NMR experiments are extremely sensitive to the local environment of the observed nuclei but also have the potential to ascertain long-range structural properties and investigate dynamic processes.[3,4] A particularly useful property of NMR is that it is isotope-selective, enabling the study of materials through many different structural "spies",[5] broadening the perspective of analysis.

The application of NMR on many relevant elements, however, is limited by the NMR sensitivity of their isotopes, often reducing its accessibility. The advancement of magic-angle spinning−dynamic nuclear polarization (MAS-DNP)[6] has significantly improved the sensitivity in many areas of NMR applications,[7−9] yet measuring nuclei with low gyromagnetic ratios or low natural abundance, such as ^{17}O, the only NMR-active isotope of oxygen with an abundance of 0.038%, can still present major challenges. Therefore, despite oxygen being ubiquitous in materials science and having NMR parameters very sensitive to the local chemical environment, NMR measurements mostly rely on isotopically enriched samples. Consequently, only a few natural abundance ^{17}O MAS NMR spectra in inorganic materials have been reported, which were achieved by utilizing long experimental times,[10] exploiting the proximity to protons for cross-polarization without[10] or with DNP,[11−15] or focusing on the surface sites via exogenous DNP.[16,17] Only recently have ^{17}O NMR spectra been acquired for proton-free bulk materials in short experimental times, either using metal-ion-based (MI)DNP[18] or, without DNP, by exploiting long transverse relaxation times with the soft CPMG (Carr−Purcell−Meiboom−Gill) approach.[19]

The difficulty in accessing ^{17}O with DNP is due to the lack of spin diffusion. Although remarkably deep spin diffusion has been reported even for low-sensitivity nuclei,[20,21] the largest enhancements in such nuclei via exogenous DNP are mainly obtained through direct polarization to the particle surface and sites close to the surface.[22,23] Various approaches have been proposed to introduce unpaired electrons to the bulk of the sample for use as endogenous hyperpolarization agents.[24−26] In particular, introducing small amounts of metal ions[27] as polarization agents in the MIDNP[28] approach has proven efficient for obtaining signal enhancements in the bulk of inorganic materials.[18,29] Still, it has been assumed that also in these approaches, efficient polarization buildup requires spin-

Received: May 18, 2020
Accepted: June 17, 2020
Published: June 17, 2020

© XXXX American Chemical Society

https://dx.doi.org/10.1021/acs.jpclett.0c01527
J. Phys. Chem. Lett. 2020, 11, 5439−5445

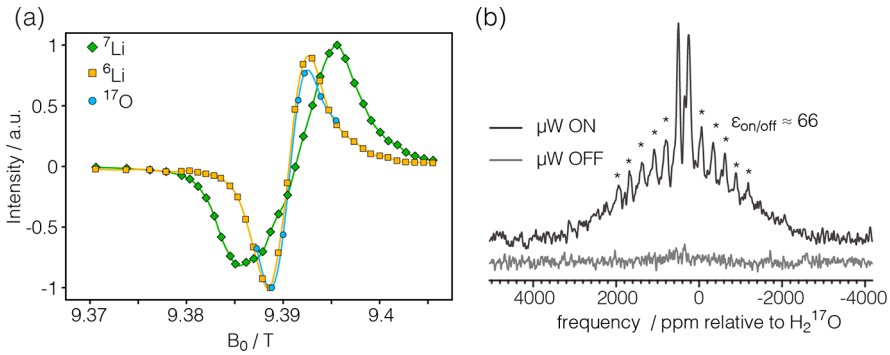

Figure 1. (a) DNP sweep profiles for ^{7}Li, ^{6}Li, and ^{17}O in Fe005LTO (^{6,7}Li) and Fe01LTO (^{17}O). (b) Natural abundance ^{17}O NMR spectra of Fe02LTO with and without μW irradiation. A recycle delay of 4.8 s was used, and a total of 1024 and 19 616 scans were acquired with and without μW irradiation, respectively. The total acquisition time was 1.37 and 26.15 h, respectively. Spectra were obtained with a Hahn echo sequence and an echo delay of 0.1 ms at 10 kHz MAS. The intensity of the spectra was scaled by the number of scans.

diffusion to spread the hyperpolarization over the sample volume.

Here we show large polarization enhancements in the absence of spin-diffusion. We have found that long nuclear relaxation times, usually one of the critical obstacles to high NMR sensitivity, can be exploited to enable large hyperpolarization throughout the entire bulk of the sample via direct polarization transfer MIDNP. Not requiring efficient spin diffusion mechanisms will mostly benefit nuclear spins with limited sensitivity due to low gyromagnetic ratios or low isotope abundance. We examine this concept by measuring ^{17}O MAS DNP NMR spectra in a series of Fe(III)-doped $Li_4Ti_5O_{12}$ (FeLTO) powders prepared via solid-state synthesis, as described in ref 29, with a varying Fe(III) mole fraction per LTO unit of x = 0.00125, 0.0025, 0.005, 0.01, and 0.02 (hereon labeled Fe00125-02LTO). These mole fractions are equivalent to a paramagnetic agent molarity ranging from 9.5 to 152 mM. Introducing small quantities of Fe(III) into the LTO structure has proven to be beneficial for its electrochemical properties as an anode material in lithium-ion batteries.[29] Because of its paramagnetic nature, it will serve as a relaxation and polarization agent to the nuclear spins.

The MAS DNP field sweep profile for ^{17}O in Fe01LTO is shown in Figure 1a, together with the field sweeps obtained for ^{6}Li and ^{7}Li (in Fe005LTO). The profile is characteristic of the solid effect, with the maximum and minimum separated by twice the nuclear Larmor frequency. A detailed analysis relating the DNP response to the electron paramagnetic resonance (EPR) spectrum in this system is given in a recent publication by our group.[29] Overlap of the ^{6}Li and ^{17}O profiles is a consequence of their similar Larmor frequencies. The possibility of heteronuclear cross-relaxation from ^{7}Li was ruled out by the clear distinction of sweep profiles and was further confirmed by the detection of identical ^{17}O spectra with and without saturation of the ^{7}Li spins during polarization buildup.

Because of the extremely low sensitivity of ^{17}O, it was only possible to obtain an NMR spectrum without microwave (μW) irradiation at the highest iron content, where the strongly reduced relaxation time allows the acquisition of a large number of scans. Figure 1b shows the ^{17}O spectra of Fe02LTO with and without μW irradiation, where a signal enhancement of $\varepsilon_{ON/OFF}$ = 66 was obtained.

Figure 2a shows the ^{17}O MIDNP MAS NMR spectra obtained with varying Fe(III) content. The addition of Fe(III) does not have any major effect on the shape of the spectrum other than a small increment of the broad component at the highest concentration. (See Figure S1.) We note the presence of two new features in the ^{17}O spectrum that had not been previously observed,[18] a very broad peak, spreading over thousands of ppm, and a narrow peak between both main peaks at 441 ppm, which likely arises from a minor oxygen environment in LTO.[18] The broad component has a very short free induction decay (FID); therefore, to be observed, it requires a Hahn echo.

The polarization buildup times, T_{BU}, obtained from fitting the saturation recovery data with a stretched exponential equation (see the Methods section), are given in Table 1 and Figure 2b and show a strong dependence on the Fe(III) content. This is a clear indication that hyperpolarization reaches beyond nuclei in immediate or close proximity to the paramagnetic center, often referred to as core nuclei.[7] No differential relaxation time was observed for different frequencies in the spectrum. (See Figure S1.) This result suggests that the spinning sidebands are not due to sites with large hyperfine couplings (which would have shorter longitudinal relaxation times), in agreement with our previous assignment of the sideband manifold to the quadrupolar satellite transitions.[18] Most surprisingly, the broad component also did not present differential T_{BU} times, as one would expect if the signal was broadened due to the proximity to a paramagnetic center. We therefore believe it is inhomogeneous in nature and arises from a distribution of quadrupolar coupling constants due to either defect sites or small local distortions.

It should be mentioned that equally good fits of the magnetization buildup curves can be obtained using two exponential functions instead of one stretched exponential function. Conceptually, two exponentials could be related to two distinct regimes, core nuclei, on one hand, and, on the other hand, bulk nuclei connected via spin diffusion. Whereas stretched exponentials arise from a continuous distribution of distances to the paramagnetic agent in the absence of spin diffusion.

To rule out the possibility of two clearly distinct regimes, a careful analysis of the line-shape evolution in the ^{6}Li spectra was performed. In such scenario, one would expect with increasing concentration a change in the relative ratio of core and bulk nuclei and a nearly constant T_1 value for the core nuclei. The fitting of ^{6}Li T_1 and T_{BU} with two exponentials does not reflect this trend. Furthermore, the vicinity to Fe(III) centers causes an observable broadening of the ^{6}Li signal. The

https://dx.doi.org/10.1021/acs.jpclett.0c01527
J. Phys. Chem. Lett. 2020, 11, 5439−5445

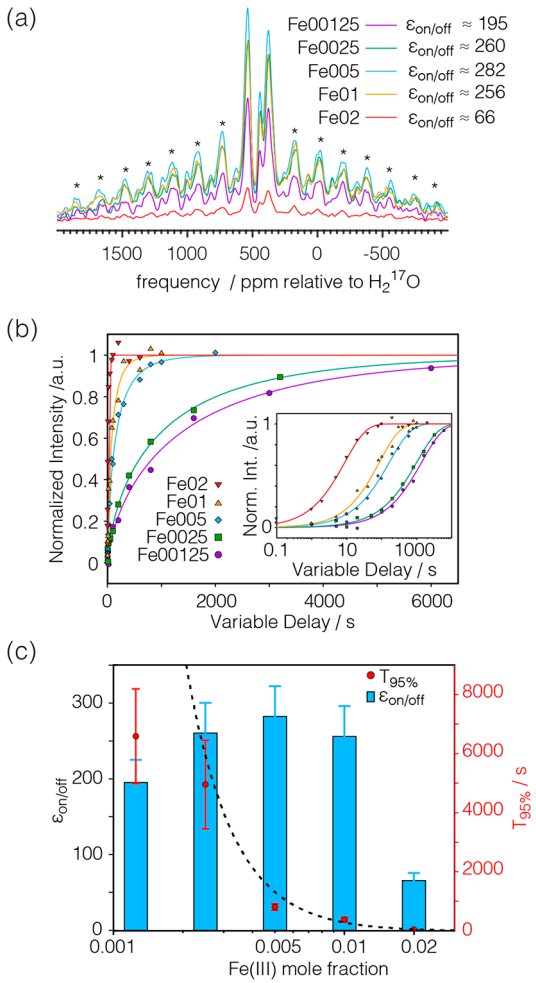

Figure 2. (a) Natural abundance ^{17}O DNP NMR spectra of iron-doped LTO. Spectra were obtained with 16 scans in all samples but Fe02LTO, which was obtained with 128 scans. (The spectrum in the figure was scaled accordingly.) All spectra were obtained with a Hahn echo sequence and an echo delay of 0.1 ms. (b) ^{17}O DNP buildup curves from integrated NMR intensities from the Hahn echo saturation recovery experiment. The inset shows the same data on a logarithmic x scale. Solid curves are best fits obtained with a stretched exponential recovery, and the fit parameters are given in Table 1. (c) Left axis: ^{17}O enhancement $\varepsilon_{ON/OFF}$, estimated taking into consideration the different quenching factors in each sample from the ^{6}Li data given in Table S3. Right axis: Buildup time of 95% of the ^{17}O polarization obtained from fits of saturation recovery measurements. The dashed line is the expected $T_{95\%}$ time from purely paramagnetic relaxation predicted from the ^{6}Li behavior. (See the Supporting Information (SI).)

spectra obtained within a saturation recovery experiment do not, however, show two distinguishable line shapes growing at different rates; instead, the line-shape evolution reflects a distribution of Lorentzian lines, with an increasing weight of narrow lines with longer relaxation delays. (See the SI for more information on the ^{6}Li measurements.)

Spin diffusion ensures that equilibrium within the nuclear spin bath is reached faster than that between individual spins and the lattice; therefore, relaxation of the magnetization occurs homogeneously throughout the entire spin system and can be described in terms of a single exponential process $\exp(-t/T_1)$.[30,31] In the absence of spin diffusion between the nuclei of interest due to MAS, large inhomogeneous broadening,[32] weak homonuclear couplings, or low isotopic abundance, relaxation in a rigid lattice is dominated by direct through-space dipolar coupling with the paramagnetic dopants. For a dilute distribution of paramagnetic centers, the magnetization reaches equilibrium following a stretched exponential behavior $\exp(-(t/T_1)^{\beta})$, with the stretched, or Kohlrausch, exponent β approaching 0.5.[33] All relaxation and buildup data measured in this study showed a stretched factor of ~0.7. The influence of the concentration, c, of paramagnetic sites on the relaxation is a further indicator of the relevance of spin diffusion to relaxation. Whereas in the presence of spin diffusion, the longitudinal relaxation time, T_1, has been shown to be linearly dependent on the inverse of the concentration of paramagnetic centers,[34,35] in its absence, T_1 depends on the dimensionality, D, of the sample as[32,36] $T_1 \propto c^{-6/D}$. Thus for a 3D solid, relaxation is expected to have an inverse squared dependence on the concentration. Analysis of the ^{6}Li relaxation and buildup data showed $T_1 \propto c^{-2.2\pm0.3}$ (Figure S3). This further confirms that in this system and under these conditions, even for the less inhomogeneously broadened and much more abundant ^{6}Li isotope (7% abundance), spin diffusion does not play a relevant role in the magnetization buildup.

The relaxation stretch factor and concentration dependence are closely related,[37] and deviation from the expected values offers the potential to monitor the homogeneity and fractal dimension of the paramagnetic site distribution.[36,38] However, this is beyond the scope of the work presented here.

To obtain the DNP enhancement, $\varepsilon_{ON/OFF}$, one would be required to measure the NMR spectrum without μW irradiation. As previously mentioned, obtaining a spectrum without DNP was only possible for the highest doped sample, Fe02LTO. By comparing the DNP signal intensity for each concentration to the Fe02LTO spectrum measured without μW irradiation, we obtain the $\varepsilon_{ON/02OFF}$ values. This comparison, however, does not consider the possibility of signal quenching due to the dopants. It was possible to quantify the quenching for the ^{6}Li NMR spectra. (See the SI.) Because of the similar gyromagnetic ratio, we expect similar quench values for ^{17}O and ^{6}Li.[39] The $\varepsilon_{ON/OFF}$ values were obtained by normalizing the intensity by the quench factor and are given in Table 1. The large uncertainties in the enhancement factors are mainly due to the lower quality of the spectrum without DNP. It is important to note, however, that the relative comparison has a much higher accuracy.

The DNP enhancement $\varepsilon_{ON/OFF}$ reaches a maximum value at a Fe(III) mole fraction of 0.005 and is nearly invariant around its maximum (Figure 2c). This plateau is reached once most ^{17}O nuclei are mainly relaxed by the paramagnetic center, allowing hyperpolarization throughout the sample. The presence of a plateau is a strong evidence that the DNP process encompasses the entire sample. An increment of dopant concentration between 0.0025 and 0.01 merely reduces the average distance between nuclei and unpaired electrons, shortening the buildup times. A further increment in concentration will ultimately shorten the electronic relaxation times, as we previously reported for this system,[29] dampening the polarization efficiency, vide infra. In Fe00125LTO, the quadrupolar relaxation mechanism has a significant contribution. (See the deviation from the dashed line in Figure 2.) Consequently, nuclei remote from the paramagnetic center will not have sufficient polarization lifetime for a large hyperpolarization. In ^{6}Li (see the SI), the maximum enhancement

https://dx.doi.org/10.1021/acs.jpclett.0c01527
J. Phys. Chem. Lett. 2020, 11, 5439−5445

Table 1. ^{17}O DNP Buildup Times and Enhancement Factors of Doped LTO for Varying Mole Fractions of Fe(III) Obtained from the Hahn Echo Saturation Recovery Experiment at 100 K, According to Equation 9[a]

$x_{Fe(III)}$	T_{BU} (s)	β	$T_{95\%}$ (s)	[S/N]/scan	$\varepsilon_{ON/02OFF}$	$\varepsilon_{ON/OFF}$
0.02	8.9 ± 0.8	0.72 ± 0.05	41 ± 6	4.5	66 ± 10	66 ± 10
0.01	86 ± 12	0.74 ± 0.08	377 ± 80	22.6	331 ± 50	256 ± 40
0.005	167 ± 16	0.70 ± 0.04	804 ± 110	28.6	377 ± 60	282 ± 40
0.0025	1011 ± 270	0.69 ± 0.06	4954 ± 1500	35.2	474 ± 70	260 ± 40
0.00125	1394 ± 290	0.71 ± 0.06	6589 ± 1600	26.5	334 ± 50	195 ± 30

[a] $T_{95\%}$ was calculated from T_{BU} and β and represents the buildup time for 95% of the polarization. Uncertainties are given as one standard deviation. The enhancement $\varepsilon_{ON/02OFF}$ represents the gain in total ^{17}O signal intensity per scan compared with Fe02LTO without μW irradiation, accounting for relaxation time to ensure the steady-state as the initial condition and sample mass. The enhancement $\varepsilon_{ON/OFF}$ was estimated taking into consideration the different quenching factors in each sample from the ^{6}Li data given in Table S3. The [S/N]/scan was obtained assuming steady-state polarization and an equal amount of 40 mg of sample.

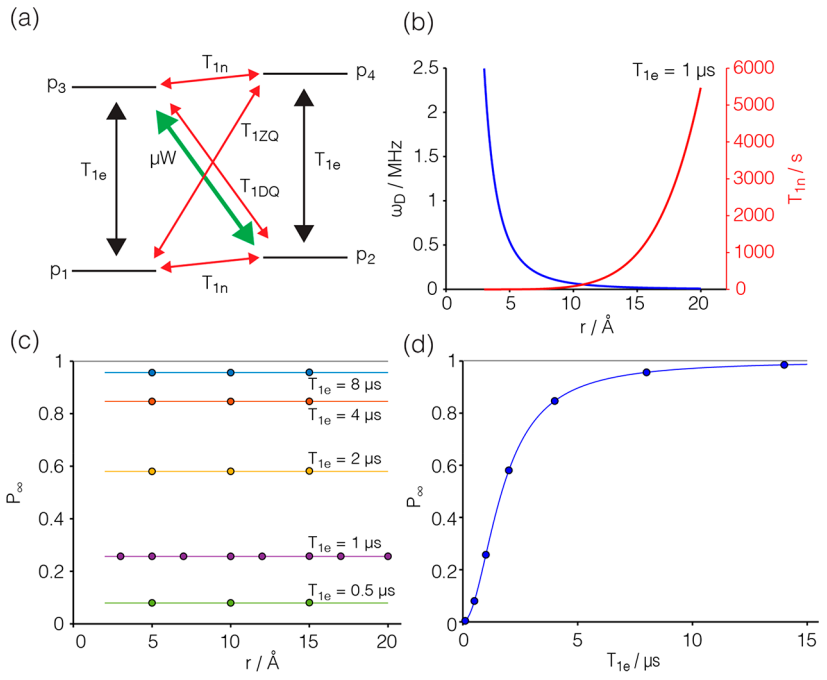

Figure 3. (a) Schematic diagram of the energy levels in a spin system consisting of one nucleus and one electron. Microwave irradiation on the double-quantum transition can lead to DNP enhancement via the solid-effect mechanism. Red arrows indicate relevant relaxation rates. (b) Distance dependence of the e−n dipolar coupling according to eq 1 (left axis, blue curve) and of the longitudinal paramagnetic relaxation time according to eq 2 (right axis, red curve). (c,d) Steady-state nuclear polarization, P_∞, relative to electronic equilibrium polarization as a function of distance (c) and electronic relaxation time (d) obtained from simulations (dots) and from the analytical expressions given in eqs 7 and 8 (lines). All calculations were done for a single electron spin $S = 1/2$ coupled to a single $I = 1/2$ nucleus with the gyromagnetic ratio of ^{17}O in a 9.4 T magnetic field at 100 K under 0.35 MHz microwave irradiation[40] on-resonance with the double-quantum transitions and assuming $T_{2e} = T_{1e}$.

plateau extends further into the low-concentration regime, as relaxation times are less affected by the much weaker quadrupolar moment.

Most importantly, these enhancements enable us to measure high-sensitivity ^{17}O NMR spectra in reduced time. The signal-to-noise ratio (S/N) per scan is given in Table 1. Of course, the paramagnetic relaxation enhancement further considerably reduces the measurement time. The ^{17}O spectrum of Fe005LTO was measured in 2 h, giving an S/N of 107. (See the SI for more details of the experimental parameters and signal intensities of all samples.)

A consequence of the experimental observation of the enhancement plateau, where the DNP efficiency is independent of the concentration, is that the steady-state nuclear hyperpolarization has to be independent of the distance between polarized nuclei and the polarizing agent. In the following discussion, we will analyze this finding from a theoretical point of view.

The DNP efficiency is mediated by the dipolar coupling, ω_D, which has an inverse cubic dependence on the distance[41]

$$\omega_D = -\frac{\mu_0}{4\pi}\frac{\hbar\gamma_e\gamma_n}{r^3} \quad (1)$$

On the contrary, nuclear longitudinal relaxation places a temporal limit on the polarization enhancement buildup. In rigid inorganic samples, the presence of fluctuating dipoles can become the main source for relaxation of nuclear magnetization.[30,34] Lowe and Tse[42] give a detailed derivation of the longitudinal relaxation considering the electronic spins as classic fluctuating dipoles and as the only source of random fluctuating fields. This allows to describe the nuclear relaxation in terms of spectral density functions in which the correlation time is given by the electronic relaxation times T_{1e} and T_{2e}. In

https://dx.doi.org/10.1021/acs.jpclett.0c01527
J. Phys. Chem. Lett. 2020, 11, 5439−5445

doped samples, where paramagnetic centers are scarce, it is unlikely that the relaxation of any nuclear spin has significant contributions from more than one electron. Considering this and taking an averaged angular value, the longitudinal relaxation expression for any nucleus, i, coupled to an electron spin, S, simplifies to[43]

$$\frac{1}{T_{1i}} = R_{1i} = \frac{2}{15}\omega_D^2 S(S+1)\left(\frac{T_{2e}}{1+T_{2e}^2(\omega_e+\omega_n)^2} + \frac{3T_{1e}}{1+T_{1e}^2(\omega_n)^2} + \frac{6T_{2e}}{1+T_{2e}^2(\omega_e-\omega_n)^2}\right) \quad (2)$$

With the assumptions that the nuclear Larmor frequency is much smaller than the electronic frequency ($\omega_n \ll \omega_e$) and $\omega_n T_{1e} \ll \omega_e T_{2e}$, the equation simplifies considerably, as the double- (DQ) and the zero-quantum (ZQ) terms (first and third in the brackets) become negligible. Figure 3 shows the distance dependence of both the dipolar coupling, which is inversely proportional to the cube of the distance, and the nuclear longitudinal relaxation time, which scales by the distance to a power of 6. In the following, we will analyze in a quantitative manner the effect of each contribution on the overall polarization enhancement. We will consider the simplest case of one single electron coupled to one single nucleus. (See Figure 3a.) Furthermore, we will assume a dilute spin bath, excluding the possibility of spin diffusion and a rigid lattice, such that the only source of nuclear relaxation arises from the paramagnetic centers.

The amount of nuclear hyperpolarization from irradiating the DQ transition will depend on the degree of saturation of the transition. Parting from phenomenological rate equations, Bloch derived analytical expressions to quantify the degree of saturation in a single spin-1/2 system under continuous μW irradiation.[44] We will describe the electron−nucleus system with analogue rate equations in an approach similar to those of Hovav et al.[45] and Smith et al.[46]

The diagonalization matrices used for diagonalization of the hyperfine interaction Hamiltonian can be used to obtain a DQ transition effective nutation frequency,[45] $\tilde{\omega}_1$

$$\tilde{\omega}_1 \approx \omega_1 \frac{C\omega_D}{2\omega_n} \quad (3)$$

where we assumed an electronic spin $S = 1/2$, with $C = \frac{3}{2}\sin\theta\cos\theta e^{-i\varphi}$ as the prefactor of the pseudosecular part of the hyperfine interaction and ω_1 the μW nutation frequency. Following the ideas introduced by the group of Vega,[45,47] the DQ and ZQ longitudinal relaxation rates were computed analogously, assuming only magnetic field fluctuations along the x direction (eq 4), and the transverse relaxation rates were assumed to be equal to the electron transverse relaxation rate ($R_{2DQ} = R_{2ZQ} = R_{2e}$).

$$R_{1DQ} = R_{1ZQ} \approx 4R_{1e}\left(\frac{C\omega_D}{4\omega_n}\right)^2 \quad (4)$$

The rate equations for populations, $p_{1,2,3,4}$, and DQ coherences, $c_{32,23}$, will have the following form

$$\frac{dp_2}{dt} = -p_2 W_\uparrow^{DQ} + p_3 W_\downarrow^{DQ} - p_2 W_\uparrow^{e} + p_4 W_\downarrow^{e} - p_2 W_\downarrow^{n} + p_1 W_\uparrow^{n} + c_{23}\frac{\tilde{\omega}_1}{2} - c_{32}\frac{\tilde{\omega}_1}{2} \quad (5)$$

and

$$\frac{dc_{32}}{dt} = p_3\frac{\tilde{\omega}_1}{2} - p_2\frac{\tilde{\omega}_1}{2} - c_{32}R_{2e} \quad (6)$$

where for the rates, W, we used the notation given by Slichter[48] with the arrows pointing toward the direction of the transitions, as shown in Figure 3a. The difference between energetically favored and nonfavored transitions was calculated from the equilibrium Boltzmann distributions.[45] The complete set of rate equations is given in the SI. Assuming that the electronic relaxation rate is much faster than any other rate, which ensures that the ratio of the energy levels connected through single-quantum electron relaxation is conserved, it is possible to derive an analytical expression for the efficiency of the saturation. (See the SI for the detailed derivation.)

$$p_2 - p_3 = \frac{(p_2 - p_3)_{eq}}{1 + \tilde{\omega}_1^2 T_{2e}[1/(2R_{1DQ} + 2R_{1n})]} \quad (7)$$

This expression assumes that the difference in population between electronic spin states is small (high-temperature approximation) but much larger than that between nuclear spin states. From this value, the nuclear polarization enhancement can be estimated and will be given as the ratio of nuclear to electron (equilibrium) polarization according to

$$P_\infty = \frac{M_{e,eq} + (p_2 - p_3)}{M_{e,eq}} \quad (8)$$

We note that eq 7 differs slightly from previously reported expressions,[45,46] as we included a total of four longitudinal relaxation paths counteracting the saturation of the DQ transition: (1) $p_2 \leftrightarrow p_3$ with the rate R_{1DQ}, (2) $p_1 \leftrightarrow p_4$ with the rate R_{1ZQ} ($\approx R_{1DQ}$), and both nuclear relaxation paths (3) $p_1 \leftrightarrow p_2$ and (4) $p_3 \leftrightarrow p_4$ with the rate R_{1n}. These paths are shown as red arrows in Figure 3a. The total longitudinal relaxation rate is obtained upon summation of the individual rates.

The most significant implication of eq 7 is that at the steady state, the polarization enhancement is de facto independent of the dipolar coupling strength. Its effects on the effective nutation field and on relaxation processes cancel each other. As a consequence, the polarization enhancement will be homogeneous throughout the sample, independent of the distance to the paramagnetic agent (also shown in Figure 3c and compared with results from quantum-mechanical simulations[45]). This is in agreement with the experimental observation of an enhancement plateau in the low-concentration regime. Of course, if R_{1n} is shortened by another relaxation mechanism, then the polarization spread from the dopant is limited. Figure 3c,d shows that small variations in the electronic relaxation times can result in a large effect on the polarization. Note that T_{2e} is unlikely to affect the nuclear relaxation but does have a huge effect on the hyperpolarization efficiency. This is in line with the experimentally observed smaller enhancement in the sample with the highest Fe(III) content, for which we reported a decrease in the electronic relaxation times.[29]

https://dx.doi.org/10.1021/acs.jpclett.0c01527
J. Phys. Chem. Lett. 2020, 11, 5439−5445

In this Letter, we presented high-quality natural abundance ^{17}O NMR spectra of the ionic conductor FeLTO using MIDNP. We show that this was made possible by the direct hyperpolarization of nuclear spins throughout the bulk of the entire sample. Variation of the Fe(III) concentration showed that the magnitude of the polarization enhancement does not depend on the distance between nucleus and polarizing agent, as long as the nuclear relaxation is dominated by the paramagnetic coupling. This finding was corroborated and explained by a careful analysis of the theoretical expressions describing the involved DNP mechanism in a simplified model and through spin dynamic simulations. These results show that MAS MIDNP NMR can be used to study the atomic structure in inorganic materials by enabling measurements of otherwise inaccessible low-sensitivity nuclei

METHODS

All NMR measurements were performed on a Bruker 9.4 T Avance-Neo spectrometer equipped with a sweep coil and a 263 GHz gyrotron system. All measurements were done at ∼100 K and at a MAS rate of 10 kHz. ^{6,7}Li measurements as well as the ^{17}O field sweeps were done using a 3.2 mm triple-resonance low-temperature (LT) DNP probe and single-pulse excitation. All other ^{17}O measurements were done using a 3.2 mm double-resonance LT-DNP probe with the Hahn echo sequence,[49] with an echo delay of 0.1 ms, equivalent to one rotor period. All measurements were done following a saturation pulse train with the recovery delays given in the SI. The radio-frequency (rf) amplitudes used were 56, 63, and 67 kHz for ^{17}O, ^{7}Li, and ^{6}Li, respectively, exciting all NMR transitions. Further specific measurement details are given in the SI. Longitudinal magnetization recovery, T_1, and hyperpolarization buildup, T_{BU}, times were determined using the saturation recovery sequence[50] and fitting with a stretched exponential function

$$M_z(t) = M_z(\infty)\cdot\left[1 - \exp\left[-\left(\frac{t}{T_{1,BU}}\right)^{\beta}\right]\right] \quad (9)$$

Processing of the NMR spectra was done with RMN 1.8.6.[51] Deconvolution of the peaks obtained from the saturation recovery experiment was done with the program deconv2D-xy.[52]

Simulations were done with a MATLAB program written by Hovav et al. presented in ref 45.

ASSOCIATED CONTENT

Supporting Information

The Supporting Information is available free of charge at https://pubs.acs.org/doi/10.1021/acs.jpclett.0c01527.

^{17}O and ^{6}Li line-shape analysis, details of used NMR experiments, ^{6}Li relaxation times, quenching and enhancement analysis, and derivation of analytical expressions (PDF)

AUTHOR INFORMATION

Corresponding Author

Michal Leskes − *Department of Materials and Interfaces, Weizmann Institute of Science, Rehovot 76100, Israel;* orcid.org/0000-0002-7172-9689; Email: michal.leskes@weizmann.ac.il

Authors

Daniel Jardón-Álvarez − *Department of Materials and Interfaces, Weizmann Institute of Science, Rehovot 76100, Israel*

Guy Reuveni − *Department of Materials and Interfaces, Weizmann Institute of Science, Rehovot 76100, Israel*

Adi Harchol − *Department of Materials and Interfaces, Weizmann Institute of Science, Rehovot 76100, Israel*

Complete contact information is available at: https://pubs.acs.org/10.1021/acs.jpclett.0c01527

Notes

The authors declare no competing financial interest.

ACKNOWLEDGMENTS

We thank Dr. Yonatan Hovav for providing the code for simulations. This research was funded by the European Research Council (MIDNP, grant no. 803024), the Planning & Budgeting Committee of the Council of High Education and the Prime Minister office of Israel, in the framework of the INREP project, and the Israel Science Foundation (grant no. 1580/17). The work was made possible in part in part by the historic generosity of the Harold Perlman family.

REFERENCES

(1) MacKenzie, K. J.; Smith, M. E. *Multinuclear Solid State Nuclear Magnetic Resonance of Inorganic Materials*; Elsevier: Burlington, VT, 2002.

(2) Pecher, O.; Carretero-González, J.; Griffith, K. J.; Grey, C. P. Materials' Methods: NMR in Battery Research. *Chem. Mater.* **2017**, *29* (1), 213−242.

(3) Böhmer, R.; Jeffrey, K. R.; Vogel, M. Solid-State Li NMR with Applications to the Translational Dynamics in Ion Conductors. *Prog. Nucl. Magn. Reson. Spectrosc.* **2007**, *50* (2−3), 87−174.

(4) Vinod Chandran, C.; Heitjans, P. Solid-State NMR Studies of Lithium Ion Dynamics Across Materials Classes. *Annu. Rep. NMR Spectrosc.* **2016**, *89*, 1−102.

(5) Eckert, H. Spying with Spins on Messy Materials: 60 Years of Glass Structure Elucidation by NMR Spectroscopy. *Int. J. Appl. Glas. Sci.* **2018**, *9* (2), 167−187.

(6) Maly, T.; Debelouchina, G. T.; Bajaj, V. S.; Hu, K.-N.; Joo, C.-G.; Mak−Jurkauskas, M. L.; Sirigiri, J. R.; van der Wel, P. C. A.; Herzfeld, J.; Temkin, R. J.; Griffin, R. G. Dynamic Nuclear Polarization at High Magnetic Fields. *J. Chem. Phys.* **2008**, *128* (5), No. 052211.

(7) Lilly Thankamony, A. S.; Wittmann, J. J.; Kaushik, M.; Corzilius, B. Dynamic Nuclear Polarization for Sensitivity Enhancement in Modern Solid-State NMR. *Prog. Nucl. Magn. Reson. Spectrosc.* **2017**, *102−103*, 120−195.

(8) Rossini, A. J. Materials Characterization by Dynamic Nuclear Polarization-Enhanced Solid-State NMR Spectroscopy. *J. Phys. Chem. Lett.* **2018**, *9* (17), 5150−5159.

(9) Rankin, A. G. M.; Trébosc, J.; Pourpoint, F.; Amoureux, J.-P.; Lafon, O. Recent Developments in MAS DNP-NMR of Materials. *Solid State Nucl. Magn. Reson.* **2019**, *101*, 116−143.

(10) Ashbrook, S. E.; Farnan, I. Solid-State ^{17}O Nuclear Magnetic Resonance Spectroscopy without Isotopic Enrichment: Direct Detection of Bridging Oxygen in Radiation Damaged Zircon. *Solid State Nucl. Magn. Reson.* **2004**, *26* (2), 105−112.

(11) Blanc, F.; Sperrin, L.; Jefferson, D. A.; Pawsey, S.; Rosay, M.; Grey, C. P. Dynamic Nuclear Polarization Enhanced Natural Abundance ^{17}O Spectroscopy. *J. Am. Chem. Soc.* **2013**, *135* (8), 2975−2978.

(12) Perras, F. A.; Kobayashi, T.; Pruski, M. Natural Abundance ^{17}O DNP Two-Dimensional and Surface-Enhanced NMR Spectroscopy. *J. Am. Chem. Soc.* **2015**, *137* (26), 8336−8339.

(13) Perras, F. A.; Chaudhary, U.; Slowing, I. I.; Pruski, M. Probing Surface Hydrogen Bonding and Dynamics by Natural Abundance, Multidimensional, ^{17}O DNP-NMR Spectroscopy. *J. Phys. Chem. C* **2016**, *120* (21), 11535−11544.
(14) Perras, F. A.; Wang, Z.; Naik, P.; Slowing, I. I.; Pruski, M. Natural Abundance ^{17}O DNP NMR Provides Precise O−H Distances and Insights into the Brønsted Acidity of Heterogeneous Catalysts. *Angew. Chem., Int. Ed.* **2017**, *56* (31), 9165−9169.
(15) Brownbill, N. J.; Gajan, D.; Lesage, A.; Emsley, L.; Blanc, F. Oxygen-17 Dynamic Nuclear Polarisation Enhanced Solid-State NMR Spectroscopy at 18.8 T. *Chem. Commun.* **2017**, *53* (17), 2563−2566.
(16) Perras, F. A.; Boteju, K. C.; Slowing, I. I.; Sadow, A. D.; Pruski, M. Direct ^{17}O Dynamic Nuclear Polarization of Single-Site Heterogeneous Catalysts. *Chem. Commun.* **2018**, *54* (28), 3472−3475.
(17) Hope, M. A.; Halat, D. M.; Magusin, P. C. M. M.; Paul, S.; Peng, L.; Grey, C. P. Surface-Selective Direct ^{17}O DNP NMR of CeO_2 Nanoparticles. *Chem. Commun.* **2017**, *53* (13), 2142−2145.
(18) Wolf, T.; Kumar, S.; Singh, H.; Chakrabarty, T.; Aussenac, F.; Frenkel, A. I.; Major, D. T.; Leskes, M. Endogenous Dynamic Nuclear Polarization for Natural Abundance ^{17}O and Lithium NMR in the Bulk of Inorganic Solids. *J. Am. Chem. Soc.* **2019**, *141* (1), 451−462.
(19) Jardón-Álvarez, D.; Bovee, M. O.; Baltisberger, J. H.; Grandinetti, P. J. Natural Abundance ^{17}O and ^{33}S Nuclear Magnetic Resonance Spectroscopy in Solids Achieved through Extended Coherence Lifetimes. *Phys. Rev. B: Condens. Matter Mater. Phys.* **2019**, *100* (14), 140103.
(20) Pinon, A. C.; Schlagnitweit, J.; Berruyer, P.; Rossini, A. J.; Lelli, M.; Socie, E.; Tang, M.; Pham, T.; Lesage, A.; Schantz, S.; Emsley, L. Measuring Nano- to Microstructures from Relayed Dynamic Nuclear Polarization NMR. *J. Phys. Chem. C* **2017**, *121* (29), 15993−16005.
(21) Björgvinsdóttir, S.; Walder, B. J.; Pinon, A. C.; Emsley, L. Bulk Nuclear Hyperpolarization of Inorganic Solids by Relay from the Surface. *J. Am. Chem. Soc.* **2018**, *140* (25), 7946−7951.
(22) Lafon, O.; Rosay, M.; Aussenac, F.; Lu, X.; Trébosc, J.; Cristini, O.; Kinowski, C.; Touati, N.; Vezin, H.; Amoureux, J.-P. Beyond the Silica Surface by Direct Silicon-29 Dynamic Nuclear Polarization. *Angew. Chem., Int. Ed.* **2011**, *50* (36), 8367−8370.
(23) Brownbill, N. J.; Lee, D.; De Paëpe, G.; Blanc, F. Detection of the Surface of Crystalline Y_2O_3 Using Direct ^{89}Y Dynamic Nuclear Polarization. *J. Phys. Chem. Lett.* **2019**, *10* (12), 3501−3508.
(24) Katz, I.; Blank, A. Dynamic Nuclear Polarization in Solid Samples by Electrical-Discharge-Induced Radicals. *J. Magn. Reson.* **2015**, *261*, 95−100.
(25) Ni, Q. Z.; Yang, F.; Can, T. V.; Sergeyev, I. V.; D'Addio, S. M.; Jawla, S. K.; Li, Y.; Lipert, M. P.; Xu, W.; Williamson, R. T.; Leone, A.; Griffin, R. G.; Su, Y. In Situ Characterization of Pharmaceutical Formulations by Dynamic Nuclear Polarization Enhanced MAS NMR. *J. Phys. Chem. B* **2017**, *121* (34), 8132−8141.
(26) Carnahan, S. L.; Venkatesh, A.; Perras, F. A.; Wishart, J. F.; Rossini, A. J. High-Field Magic Angle Spinning Dynamic Nuclear Polarization Using Radicals Created by γ-Irradiation. *J. Phys. Chem. Lett.* **2019**, *10* (17), 4770−4776.
(27) Corzilius, B.; Smith, A. A.; Barnes, A. B.; Luchinat, C.; Bertini, I.; Griffin, R. G. High-Field Dynamic Nuclear Polarization with High-Spin Transition Metal Ions. *J. Am. Chem. Soc.* **2011**, *133* (15), 5648−5651.
(28) Chakrabarty, T.; Goldin, N.; Feintuch, A.; Houben, L.; Leskes, M. Paramagnetic Metal-Ion Dopants as Polarization Agents for Dynamic Nuclear Polarization NMR Spectroscopy in Inorganic Solids. *ChemPhysChem* **2018**, *19* (17), 2139−2142.
(29) Harchol, A.; Reuveni, G.; Ri, V.; Thomas, B.; Carmieli, R.; Herber, R. H.; Kim, C.; Leskes, M. Endogenous Dynamic Nuclear Polarization for Sensitivity Enhancement in Solid-State NMR of Electrode Materials. *J. Phys. Chem. C* **2020**, *124* (13), 7082−7090.
(30) Bloembergen, N. On the Interaction of Nuclear Spins in a Crystalline Lattice. *Physica* **1949**, *15* (3−4), 386−426.
(31) Bakhmutov, V. I. Strategies for Solid-State NMR Studies of Materials: From Diamagnetic to Paramagnetic Porous Solids. *Chem. Rev.* **2011**, *111* (2), 530−562.
(32) Bodart, J. R.; Bork, V. P.; Cull, T.; Ma, H.; Fedders, P. A.; Leopold, D. J.; Norberg, R. E. Recovery of Nuclear Magnetization under Extreme Inhomogeneous Broadening. *Phys. Rev. B: Condens. Matter Mater. Phys.* **1996**, *54* (21), 15291−15298.
(33) Tse, D.; Hartmann, S. R. Nuclear Spin-Lattice Relaxation Via Paramagnetic Centers Without Spin Diffusion. *Phys. Rev. Lett.* **1968**, *21* (8), 511−514.
(34) Blumberg, W. E. Nuclear Spin-Lattice Relaxation Caused by Paramagnetic Impurities. *Phys. Rev.* **1960**, *119* (1), 79−84.
(35) Tse, D.; Lowe, I. J. Nuclear Spin-Lattice Relaxation in CaF_2 Crystals via Paramagnetic Centers. *Phys. Rev.* **1968**, *166* (2), 292−302.
(36) Devreux, F.; Boilot, J. P.; Chaput, F.; Sapoval, B. NMR Determination of the Fractal Dimension in Silica Aerogels. *Phys. Rev. Lett.* **1990**, *65* (5), 614−617.
(37) Devreux, F.; Malier, L. Nonexponentiality and Thermal Variation of Nuclear Relaxation in Glasses. *Phys. Rev. B: Condens. Matter Mater. Phys.* **1995**, *51* (17), 11344−11347.
(38) Sen, S.; Stebbins, J. F. Phase Separation, Clustering, and Fractal Characteristics in Glass: A Magic-Angle-Spinning NMR Spin-Lattice Relaxation Study. *Phys. Rev. B: Condens. Matter Mater. Phys.* **1994**, *50* (2), 822−830.
(39) Li, W.; Zhang, Q.; Joos, J. J.; Smet, P. F.; Schmedt auf der Günne, J. Blind Spheres of Paramagnetic Dopants in Solid State NMR. *Phys. Chem. Chem. Phys.* **2019**, *21* (19), 10185−10194.
(40) Mentink-Vigier, F.; Barra, A.-L.; van Tol, J.; Hediger, S.; Lee, D.; De Paëpe, G. De Novo Prediction of Cross-Effect Efficiency for Magic Angle Spinning Dynamic Nuclear Polarization. *Phys. Chem. Chem. Phys.* **2019**, *21* (4), 2166−2176.
(41) Grandinetti, P. J.; Ash, J. T.; Trease, N. M. Symmetry Pathways in Solid-State NMR. *Prog. Nucl. Magn. Reson. Spectrosc.* **2011**, *59* (2), 121−196.
(42) Lowe, I. J.; Tse, D. Nuclear Spin-Lattice Relaxation via Paramagnetic Centers. *Phys. Rev.* **1968**, *166* (2), 279−291.
(43) Bertini, I.; Luchinat, C.; Parigi, G.; Ravera, E. *NMR of Paramagnetic Molecules*, 2nd ed.; Elsevier: Boston, 2017.
(44) Bloch, F. Nuclear Induction. *Phys. Rev.* **1946**, *70* (7−8), 460−474.
(45) Hovav, Y.; Feintuch, A.; Vega, S. Theoretical Aspects of Dynamic Nuclear Polarization in the Solid State − The Solid Effect. *J. Magn. Reson.* **2010**, *207* (2), 176−189.
(46) Smith, A. A.; Corzilius, B.; Barnes, A. B.; Maly, T.; Griffin, R. G. Solid Effect Dynamic Nuclear Polarization and Polarization Pathways. *J. Chem. Phys.* **2012**, *136* (1), No. 015101.
(47) Kundu, K.; Mentink-Vigier, F.; Feintuch, A.; Vega, S. DNP Mechanisms. *eMagRes.* **2019**, *8* (3), 295−338.
(48) Slichter, C. P. *Principles of Magnetic Resonance*, 1st ed.; Harper & Row: New York, 1963.
(49) Hahn, E. Spin Echoes. *Phys. Rev.* **1950**, *80* (4), 580−594.
(50) Markley, J. L.; Horsley, W. J.; Klein, M. P. Spin-Lattice Relaxation Measurements in Slowly Relaxing Complex Spectra. *J. Chem. Phys.* **1971**, *55* (7), 3604−3605.
(51) PhySy, Ltd. *RMN*, version 1.8.6. www.physyapps.com (accessed 27th July 2019).
(52) Jardón-Álvarez, D.; Schmedt auf der Günne, J. Reduction of the Temperature Gradients in Laser Assisted High Temperature MAS NMR. *Solid State Nucl. Magn. Reson.* **2018**, *94*, 26.

https://dx.doi.org/10.1021/acs.jpclett.0c01527
J. Phys. Chem. Lett. 2020, 11, 5439−5445